

Original Research Article

Uncovering the dynamics of a circadian-dopamine model influenced by the light–dark cycle

Ruby Kim^{*}, Thomas P. Witelski

Department of Mathematics, Duke University, Durham, NC, USA

ARTICLE INFO

Keywords:

Circadian rhythms
Dopamine
Quasiperiodicity
Entrainment

ABSTRACT

The neurotransmitter dopamine (DA) is known to be influenced by the circadian timekeeping system in the mammalian brain. We have previously created a single-cell differential equations model to understand the mechanisms behind circadian rhythms of extracellular DA. In this paper, we investigate the dynamics in our model and study different behaviors such as entrainment to the 24-hour light–dark cycle and robust periodicity versus decoupling, quasiperiodicity, and chaos. Imbalances in DA are often accompanied by disrupted circadian rhythms, such as in Parkinson's disease, hyperactivity, and mood disorders. Our model provides new insights into the links between the circadian clock and DA. We show that the daily rhythmicity of DA can be disrupted by decoupling between interlocked loops of the clock circuitry or by quasiperiodic clock behaviors caused by misalignment with the light–dark cycle. The model can be used to further study how the circadian clock affects the dopaminergic system, and to help develop therapeutic strategies for disrupted DA rhythms.

1. Introduction

The mammalian circadian clock is a network of genes and proteins in the suprachiasmatic nucleus (SCN) that drives 24-h oscillations in important physiological functions such as the sleep–wake cycle, hormone and neurotransmitter regulation, and physical activity [1–3]. The circadian clock circuitry is highly complex and consists of interlocked feedback loops. Oscillations are primarily driven by BMAL1-CLOCK heterodimers, which activate the transcription of Period (PER) and Cryptochrome (CRY) genes, which then encode proteins that inhibit BMAL1-CLOCK [4]. An important secondary loop consists of orphan nuclear receptors REV-ERBs and retinoic acid-related orphan receptors (RORs), which are downstream products of the circadian clock and modulate the Brain and Muscle ARNT-Like 1 (Bmal1) gene to reciprocally influence circadian rhythms [5,6].

Many mathematical models have been created to study circadian rhythms at the single cell level. Forger and Peskin [7] developed a highly detailed and robust model of the circadian clock circuitry including its responses to light perturbations. Leloup and Goldbeter [8] created a model of mammalian circadian rhythms which they used to predict clock behavior in different light–dark conditions. Hong, Conrad, and Tyson [9] used a simple negative feedback model to theorize a mechanism for temperature compensation. In animals with variable body temperature, the circadian clock remains robust despite temperature-related changes to chemical rates. Additionally, mathematical models have been used to study synchronization of circadian

rhythms across different cells. Garcia-Ojalvo, Elowitz, and Strogatz [10] created a mathematical model of intercellular signaling in coupled oscillators, and Strogatz [11] provides a detailed review of the long history of coupled oscillator models.

While the molecular machinery of the mammalian circadian clock is well established, the clock is capable of non-oscillatory or oscillatory but non-periodic behaviors that are not fully understood. Mice with genetic perturbations may show arrhythmic activity patterns [12–15] and disruptions to the 24-h light–dark cycle result in oscillatory behaviors that lose periodicity [16]. Such behaviors have important clinical implications as they are strongly linked to a host of health conditions, including metabolic and cardiac dysfunction [17]. Several mathematical studies have previously explored non-periodic dynamics in clock models. In [18], Gonze and Goldbeter studied quasiperiodicity and chaos in a model for circadian rhythms in *Neurospora* and explored the influences of the waveform and amplitude of light input on entrained versus non-periodic behaviors. In a model for circadian rhythms in *Drosophila*, Kurosawa and Goldbeter [19] have shown that quasiperiodic behaviors occur under the light–dark cycle when the natural period of the clock is sufficiently far from 24 h. Several other circadian models have also displayed quasiperiodic or chaotic dynamics [20,21] but have not explored these behaviors in detail. In this paper, we investigate periodic and non-periodic behaviors in a mammalian clock model and study their influences on an important neurotransmitter.

^{*} Corresponding author.

E-mail address: rubykim@math.duke.edu (R. Kim).

There is evidence that the neurotransmitter dopamine (DA) is modulated by the circadian clock, but not much is known about the underlying mechanisms. DA is involved with learning, motivation, and reward [22,23], and is associated with neurological conditions such as Parkinson's disease, schizophrenia, and hyperactivity [24–26]. Many individuals with DA-related conditions also display disrupted circadian rhythms [27–29]. Ikeda et al. [30] have shown that REV-ERBs and RORs regulate the expression of dopamine D3 receptors (DRD3). Chung et al. [31] and Sleipness et al. [32] measured diurnal variations in tyrosine hydroxylase (TH), the rate-limiting enzyme in DA synthesis. Hampf et al. [33] showed that monoamine oxidase (MAO), which catabolizes DA, is controlled by clock proteins. Finally, extracellular DA has been shown to vary diurnally in the rat brain [34]. In 2021, R. Kim (an author of this paper) and M. Reed [35] created a mathematical model of the circadian clock and its downstream influences on dopaminergic variables, based on experiments in [30,31,33]. This mathematical model was then connected to the extant model of DA synthesis and release by Best et al. [36]. The model predictions of extracellular DA were consistent with data in [34], giving strong evidence that the mechanisms proposed by experimentalists [30,31,33] are sufficient to explain diurnal variation in extracellular DA.

In this paper, we use a reduced version of the previous model [35] to capture the essential clock dynamics and perform a thorough mathematical analysis; see Fig. 1 for a schematic. As in the original model, the mathematical model in this paper consists of three interlocking systems: (1) the core circadian clock which consists of BMAL1-CLOCK (BC) and the successively phosphorylated Period proteins ($\{P_i\}_{i=1}^4$); (2) the secondary feedback loop involving REV-ERBs (REV), RORs (ROR), BC , and $Bmal1$ (S); and (3) the downstream influences on tyrosine hydroxylase (TH) and monoamine oxidase (MAO) in the dopaminergic system. The reduced model displays characteristic features of the circadian clock and describes the influences of the circadian clock on dopaminergic variables. Details of the differential equations and parameters are included in the Methods section.

Throughout this paper, we highlight the different clock phenotypes generated by the mathematical model, how they are influenced by light and parameter variation, and their connections to experimental observations. In Section 3, we characterize regular diurnal rhythms in our circadian clock model and identify bifurcations in a biologically motivated range of parameters. In Section 4, we explore how protein sequestration in the model gives rise to piecewise-smooth dynamics, and we find conditions that lead to decoupling of BC and S . While circadian rhythms persist in all other clock variables, we show that this decoupling behavior could have harmful health outcomes by disrupting DA rhythmicity. In Section 5, we demonstrate that low light amplitudes result in a narrow parameter range for healthy rhythms, with quasiperiodic behaviors below and above that range. As light amplitude is increased, the range for healthy rhythms expands. Finally, in Section 6 we show that sufficiently strong light variation leads to period homeostasis and eliminates quasiperiodicity in the parameter regime of interest.

2. Methods

The mathematical model studied in this paper consists of differential equations describing the core circadian clock, a secondary feedback loop, and downstream dopaminergic variables. In Section 2.1, we describe the reduced model equations for the circadian clock and secondary feedback loop. In Section 2.2, we present the model equations for TH and MAO, which are influenced by the circadian clock, and in Section 2.3 we describe how we connect our results to an extant model [36] to simulate daily variation in extracellular DA.

2.1. Model development

A schematic diagram of the reduced mathematical model is provided in Fig. 1. The core circadian clock consists of variables $\{P_i\}_{i=1}^4$ and BC . As in the original model, the production term for P_1 depends on the amount of free BC after sequestration by P_4 , which is $f_0(BC, P_4)$ in this paper. In the original model, the core circadian clock included the repression of BC -mediated transcription by the clock protein CRY. In this model, we have omitted this second form of repression.

Circadian rhythms are primarily driven by a negative feedback loop, involving inhibition of BC by P_4 through protein sequestration. A function for protein sequestration was derived in [37] and used in the circadian models by Kim and Forger [38–40] to describe the sequestration of a protein P by an inhibitor I , with dissociation constant $D \ll 1$. The function is

$$f(P, I, D) = \frac{1}{2} \left(P - I - D + \sqrt{(P - I - D)^2 + 4DP} \right), \quad (1)$$

where $f(P, I, D)$ is the concentration of free P not bound to I . Note that in our original model [35] and in [38–40], the protein sequestration function is expressed as a ratio of free P to total P . In Eq. (1), $f(P, I, D)$ is the concentration of free P . We simplify Eq. (1) by taking $D \rightarrow 0$, so the protein sequestration term in this model is

$$f_0(P, I) = \frac{P - I + |P - I|}{2} = \begin{cases} P - I & P > I \\ 0 & P \leq I. \end{cases} \quad (2)$$

Light increases the expression of Per genes in the SCN [1,41,42]. As in the original model, we have modeled light input by adjusting the production rate of P_1 to vary diurnally. In many experiments, light-dark conditions are created by switching lights on/off instead of gradually adjusting light intensity. We chose to use a step function $L(t, x)$ to model the impact of light at time t , with x as percent change of the production rate of P_1 (Eq. (3)). As a result, the mathematical model with light input is in one of two states (light vs dark) depending on the Zeitgeber Time (ZT). ZT is a unit of time that corresponds to the 12:12 light-dark cycle, with ZT0 indicating beginning of light and ZT12 indicating beginning of dark. The light function is

$$L(t, x) = \begin{cases} 1 + x & t \bmod 24 < 12 \\ 1 - x & \text{otherwise.} \end{cases} \quad (3)$$

In the free running model without light input, we let $x = 0$ so that $L = 1$. All other production and degradation terms are linear. BC production is dependent on S , which can be thought of as $Bmal1$. The reduced model equations for the core circadian clock are

$$\frac{dP_1}{dt} = r_1 L(t, x) f_0(BC, P_4) - r_2 P_1, \quad (4a)$$

$$\frac{dP_2}{dt} = r_2 P_1 - r_3 P_2, \quad (4b)$$

$$\frac{dP_3}{dt} = r_3 P_2 - r_4 P_3, \quad (4c)$$

$$\frac{dP_4}{dt} = r_4 P_3 - d_4 P_4, \quad (4d)$$

$$\frac{dBC}{dt} = \beta_{bc} S - d_{bc} BC. \quad (4e)$$

The core circadian clock is linked to a secondary feedback loop via BC , which activates the transcription of REV and ROR , which then modulate S . The secondary feedback loop consists of variables S , REV , and ROR . REV and ROR are known to compete for binding to the $Bmal1$ (S) promoter, with REV acting as a repressor and ROR as an activator [5,43]. Ikeda et al. [30] found that REV and ROR peak at the same time, with a net effect of inhibition near the peaks and activation away from the peaks. We chose to model the competing effects of REV and ROR on S with a simple term $\alpha f_0(S, REV)ROR$. The term $f_0(S, REV)$ is the amount of free S after REV binding.

Light input enters the model as a factor multiplying the r_1 rate constant in Eq. (4a). As a periodic time-dependent coefficient in the

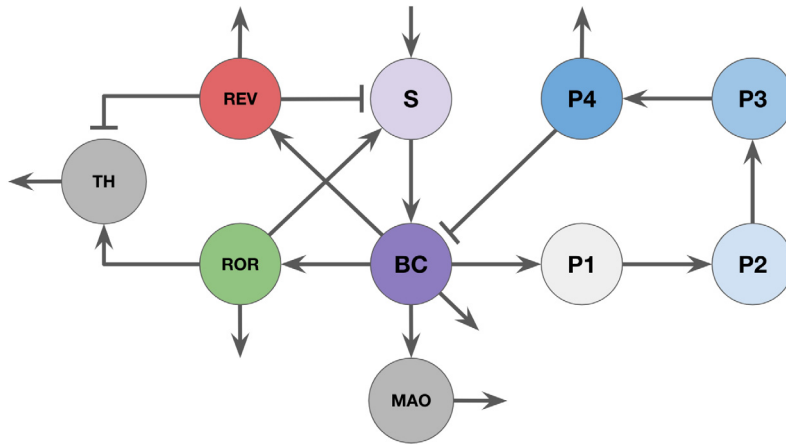


Fig. 1. Schematic diagram of the circadian clock model. The protein complex BMAL1-CLOCK (BC) promotes the production of PER, which goes through multiple phosphorylation steps ($\{P_i\}_{i=1}^4$). Phosphorylated PER inhibits its own production by inhibiting BC . A secondary loop consists of REV and ROR , which are activated by BC and reciprocally modulate Bmal1 (S), a precursor to BC . Arrows facing outwards denote degradation. The downstream dopaminergic variables TH and MAO are modulated by REV , ROR , and BC . TH is the rate-limiting enzyme in DA synthesis and MAO is involved in DA degradation.

system, mathematically this is called parametric forcing [44,45]. For $x \geq 0$, periodic solutions become non-generic as the 24-h forcing cycle can interact with the natural period of the unforced system (to be called the “free running model”) to generate oscillatory but non-periodic behaviors (quasiperiodic solutions). Later we will show that for strong light input (sufficiently large x), solutions of the system can become periodic on a 24-h cycle, sometimes called entrainment or frequency locking.

As in Eq. (4a) for P_1 , the production terms of REV and ROR are dependent on $f_0(BC, P_4)$, the amount of free BC . The reduced model equations for the secondary loop are

$$\frac{dS}{dt} = \beta + \alpha f_0(S, REV)ROR - d_s S, \quad (4f)$$

$$\frac{dREV}{dt} = r_{rev} f_0(BC, P_4) - d_{rev} REV, \quad (4g)$$

$$\frac{dROR}{dt} = r_{ror} f_0(BC, P_4) - d_{ror} ROR. \quad (4h)$$

2.2. Downstream dopaminergic variables

Tyrosine hydroxylase (TH) and monoamine oxidase (MAO) are the downstream dopaminergic variables in the mathematical model; see Fig. 1. We use the mathematical model to predict the daily time series of TH and MAO , which we then connect to the extant model of DA by Best et al. [36] to predict the circadian rhythms of extracellular DA (eDA).

TH is the rate-limiting enzyme in DA synthesis. TH varies diurnally in experiments and is coordinately modulated by REV and ROR , with REV inhibiting and ROR activating TH [2,31,32]. The differential equation for the circadian clock’s influence on TH is exactly the same as in the original model [35], and is

$$\frac{dTH}{dt} = b_{th} + \mathcal{R}(TH, REV) + \mathcal{A}(TH, REV, ROR) - d_{th} TH \quad (5)$$

where

$$\mathcal{R}(TH, REV) = \frac{\rho_{th}}{\left(1 + k_{th} \left(1 - \frac{f(TH, REV, \epsilon_{th})}{TH}\right)\right)^{n_{th}}}, \quad (6)$$

$$\mathcal{A}(TH, REV, ROR) = \alpha_{th} \frac{f(TH, REV, \epsilon_{th})}{TH} \frac{ROR}{ROR + \kappa_{th}}. \quad (7)$$

MAO is an enzyme essential for DA degradation, and is thought to be activated by BC [2,33]. As in the original model [35], the production rate of MAO is dependent on the amount of free BC . In the reduced model in this paper, free BC is $f_0(BC, P_4)$ where f_0 is the function in Eq. (2). The differential equation for MAO is

$$\frac{dMAO}{dt} = r_m f_0(BC, P_4) - d_m MAO. \quad (8)$$

2.3. Extant DA model

We connect our TH and MAO results to an existing mathematical model of DA synthesis and release by Best et al. [36]. The schematic diagram of the DA model is provided in Fig. 2 and shows the reactions described by the model equations. TH converts tyrosine (tyr) into L-3,4-dihydroxyphenylalanine (l-dopa), which is then decarboxylated to cytosolic dopamine (cda). Cytosolic dopamine is packaged into vesicles and released into the extracellular space as extracellular dopamine (eda). In this paper, the variable name for extracellular dopamine is eDA . MAO catabolizes cytosolic and extracellular DA. We save the time series produced in our model for TH and MAO (relative to their peak values) and multiply these variations to the velocities of the TH and MAO reactions respectively in the equations from [36] to generate circadian rhythms in DA. Full details of the DA model including the 9 differential equations are in [36].

In Fig. 3, the eDA model curve (yellow) under a 12:12 light-dark cycle is 24-h periodic, with eDA peaks shortly following TH (solid gray curve) peaks, and eDA decreasing when MAO (dashed gray curve) is elevated. This relationship between eDA , TH , and MAO is consistent with the role of TH in DA synthesis and the role of MAO in DA catabolism. The original model [35] was used to predict eDA variation in the rat striatum, which corresponded well with data from [34]. We remark that the interest of this paper is to use a simple model to understand the potential DA dynamics resulting from circadian clock disruptions, and not to predict exact time courses in any specific mammal or region of the brain. In Sections 4 and 5, we characterize different types of clock behavior and their downstream effects on extracellular DA rhythmicity.

2.4. Parameter selection and computational methods

All computations were done with the parameter values listed in Table 1 unless otherwise specified. The parameters for this reduced model were selected with three major goals for model variables. The first two goals were to obtain reasonable amplitudes of circadian variation and accurate phase relationships between model variables suggested by free running experiments and previous models [35,38,46]. The third goal was to achieve a period close to 23.5 h as in mouse experiments without light input [3]. As no changes were made to the differential equation for TH , parameter values appearing in Eq. (5) were kept the same as in the original model [35]. We point to the Methods in [35] for a detailed discussion of parameter selection.

All computations in the Results section were performed in MATLAB. In Section 3, we demonstrate the circadian rhythms generated

Table 1
Parameter values used in the mathematical model.

Par.	Val.	Description	Sources
x	0.3	Amplitude of the light function	[35,38]
r_1	0.5	Production constant of P_1 proportional to net effect of light and activation by free BC	[3,35,38,46]
r_2	0.2	P_1 phosphorylation rate	[3,35,38,46]
r_3	0.2	P_2 phosphorylation rate	[3,35,38,46]
r_4	0.2	P_3 phosphorylation rate	[3,35,38,46]
d_4	0.2	Degradation rate of P_4	[3,35,38,46]
β_{bc}	0.5	Production rate of BC from S	[3,35,38,46]
d_{bc}	0.3	Degradation rate of BC	[3,35,38,46]
β	0.5	Basal production rate of S	[30,35,38]
α	0.5	Production rate of S proportional to net effect of inhibition by REV and activation by ROR	[30,35,38]
d_s	0.5	Degradation rate of S	[30,35,38]
r_{rev}	0.3	Production rate of REV proportional to free BC	[30,35]
d_{rev}	0.2	Degradation rate of REV	[30,35]
r_{ror}	0.3	Production rate of ROR proportional to free BC	[30,35]
d_{ror}	0.2	Degradation rate of ROR	[30,35]
b_{th}	0	Basal production rate of TH	[31,35]
d_{th}	5.6	Degradation rate of TH	[31,35]
ρ_{th}	1	Strength of TH repression as a function of percent TH bound to REV	[31,35]
k_{th}	1	Coefficient in TH repression term as a function of percent TH bound to REV	[31,35]
ϵ_{th}	0.3	Dissociation constant between TH and REV	[31,35]
n_{th}	1	Exponent in TH repression term as a function of percent TH bound to REV	[31,35]
α_{th}	3.7	Strength of activation of free TH (not bound to REV) by ROR	[31,35]
κ_{th}	1	Constant in TH activation term	[31,35]
r_m	3	Production rate of MAO proportional to free BC	[33,35]
d_m	0.02	Degradation rate of MAO	[33,35]

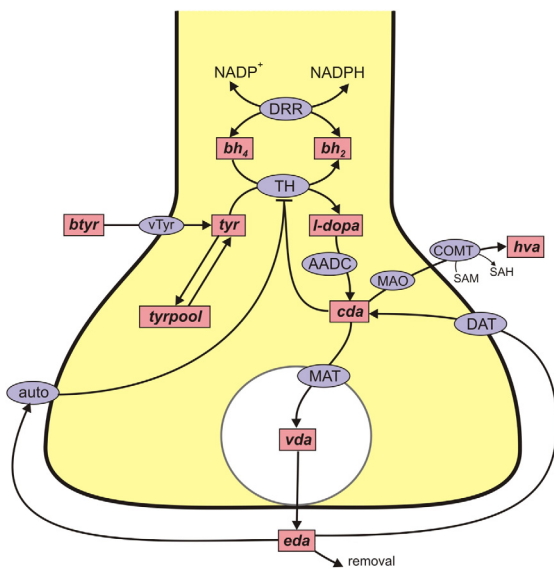


Fig. 2. (B) Schematic diagram of the extant DA model. The model in this paper generates circadian rhythms of TH and MAO . We connect our model to the extant model of dopamine synthesis and release by Best et al. [36] to predict circadian variation in extracellular DA. Rectangular boxes indicate substrates and blue ellipses indicate enzymes or transporters. Full details of the DA model are in [36]. Abbreviations: btyr, blood tyrosine; bh2, dihydrobiopterin; bh4, tetrahydrobiopterin; tyr, tyrosine; l-dopa, 3,4-dihydroxyphenylalanine; cda, cytosolic dopamine; vda, vesicular dopamine; eda, extracellular dopamine; hva, homovanillic acid; tyrpool, the tyrosine pool; vTyr, neutral amino acid transporter; DRR, dihydrobiopterin reductase; TH, tyrosine hydroxylase; AADC, aromatic amino acid decarboxylase; MAT, vesicular monoamine transporter; DAT, dopamine transporter; auto, D2 dopamine auto receptors; MAO monoamine oxidase; COMT, catecholamine O-methyl transferase.

by the mathematical model in both free running and 12:12 light-dark conditions. Numerical solutions were computed using MATLAB's

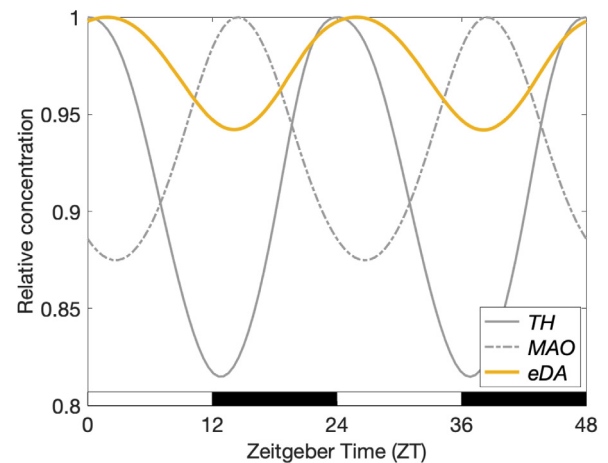


Fig. 3. Circadian rhythms of downstream dopamine. The reduced mathematical model predicts diurnal variation in TH (solid gray curve) as a result of modulation by REV and ROR , and in MAO (dashed gray curve) as a result of activation by BC . Consistent with the original model [35], TH and MAO are nearly antiphasic. The 24-h periodic oscillations of TH and MAO are used to model circadian rhythms in extracellular DA (eDA , yellow curve). As we would expect, extracellular DA peaks shortly after TH peaks, and drops when MAO rises.

ode45 and ode23s routines. When solutions converged to a limit cycle, we computed period as the time separation between P_2 peaks. In Section 3.2, we identify and discuss Hopf bifurcation points in the core circadian clock under free running and constant light conditions. We used Matcont, a numerical continuation package in MATLAB, to compute bifurcation diagrams after smoothing the piecewise function $f_0(P, I)$ as $f(P, I, D)$ from Eq. (1) with dissociation constant $D = 1 \times 10^{-16}$ [38] in the equations for P_1 , S , REV , and ROR .

We chose to focus on the parameters r_1 and d_{bc} , where r_1 determines the rate of production of P_1 and d_{bc} is the degradation rate of the activator BC . Each parameter was varied by at least 25%, since it

is known that enzyme expression levels vary by about 25% between individuals of the same species [47–49]. In the model, we treat this range as “normal”. In Section 4, we study the different dynamics that arise out of the protein sequestration term in Eq. (2), depending on the amount of inhibitor relative to the amount of protein it sequesters. Experiments in [50] demonstrate that protein sequestration can generate ultrasensitive behavior depending on the abundance of an inhibitor. In Section 5, we present some quasiperiodic and chaotic behaviors resulting from parameter and light perturbations. Numerical solutions for varying r_1 are obtained using MATLAB’s ode45, and are used to create Poincaré sections. Lyapunov exponents to identify quasiperiodicity or chaos were computed numerically using the algorithm developed by Wolf et al. [51]. Finally, in Section 6, we discuss period homeostasis. Period is again computed using the time separation between peaks, and secondary period is computed by first performing interpolation of P_2 time series peaks, then finding the time separation between the interpolated curve’s peaks.

3. Circadian oscillations and Hopf bifurcations

3.1. Clock rhythms

The circadian clock variables in this mathematical model are $\{P_i\}_{i=1}^4$ where i is the number of phosphorylations, BC , S , REV , and ROR ; see Fig. 1. The protein complex BMAL1-CLOCK, BC , promotes the transcription of *Per* genes. *PER* proteins, P_1 , are transported to the cytosol where they undergo multiple phosphorylation steps. Then, phosphorylated *PER*, P_4 , binds with the protein *CRY* to re-enter the nucleus and inhibit activation by BC . In the secondary loop, BC activates REV and ROR . These proteins reciprocally modulate S or *Bmal1*, a precursor to BC , with REV inhibiting S and ROR activating S . The results of these interlocked feedback loops can be seen in Fig. 4, and the proteins’ relative phase relationships and amplitudes are consistent with our original model.

The free running model is oscillatory with period 23.5 h, as in mouse experiments without light input [3]; see Fig. 4B. In the light-entrained model with $x = 0.3$, period length is 24 h; see Fig. 4D. S peaks during the beginning of subjective night, and *PER*, P_2 , peaks in the middle of the night when mice are active, as in [52]. In the model, increasing the light variation x increases the circadian amplitude which is consistent with experiments in [53].

Healthy, robust circadian rhythms rely on balanced stoichiometry between circadian activators and repressors [38,54]. S is activated by ROR and inhibited by REV , and its rate equation has a simple form which models these reciprocal influences well. However, ROR and REV , the basal production rate β , and the degradation term $d_s S$ need to be balanced in Eq. (4f) to stabilize S . The mathematical model is quite robust as we will see in Section 6, but one must use reasonable initial conditions. In the Appendix, we analyze the conditions under which S can destabilize.

3.2. Hopf bifurcations

Previously, the original model [35] successfully predicted circadian rhythms in dopaminergic variables [30,31,33,34]. We use the reduced model in this paper to show how variations in particular parameters affect the circadian clock’s dynamics. The parameter r_1 can be thought of as the transcription rate of *PER*. Variation in r_1 in the free running model leads to a supercritical Hopf bifurcation at $r_1 = 0.3$; see Fig. 5A. Steady state values for $r_1 < 0.3$ are computed in Section 4.1. In Fig. 5, the green shaded regions span 25% below and 25% above the original parameter value and indicate the parameter range of interest as described in the Methods. Solid orange curves indicate the bounds of stable limit cycles, which span across the entire parameter range of interest. A subcritical Hopf bifurcation occurs at $r_1 = 0.8$, where a branch of equilibria becomes stable and an unstable limit cycle appears.

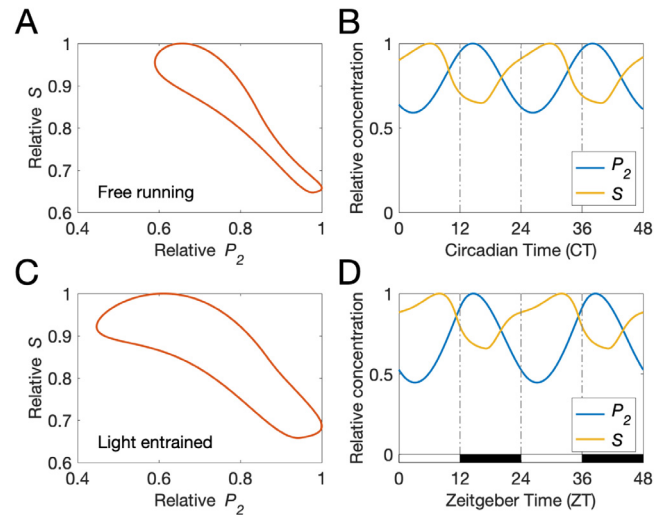


Fig. 4. Model clock oscillations in free running conditions and 12:12 light-dark conditions. Protein concentrations are plotted relative to their maximum. In free running conditions, the period is 23.5 h and relative P_2 has an amplitude of 0.41 (panels A–B). In 12–12 light–dark conditions, the period is 24 h and the amplitude of P_2 is 0.55 (panels C–D).

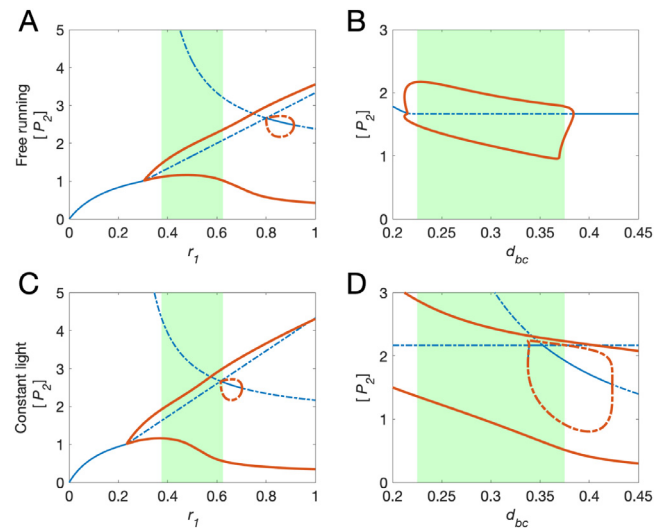


Fig. 5. One-parameter bifurcation diagrams of the free running model with $x = 0$ (panels A–B) and model under constant light (panels C–D). Constant light means lights on for all t , or $L = 1.3$ in Eq. (4a). Green shaded regions indicate parameter regions of interest, 25% below and 25% above original parameter values ($r_1 = 0.5$ and $d_{bc} = 0.3$). Blue curves indicate equilibrium points and orange curves indicate the bounds of limit cycles. Stable branches of solutions are solid and unstable branches are dashed. In the free running model there is a Hopf bifurcation at $r_1 = 0.3$ (panel A), and in the model with constant light there is a Hopf bifurcation at $r_1 = 0.23$ (panel C).

At $r_1 = 0.913$, the unstable limit cycle vanishes and the branch of equilibria becomes unstable. Not only are the limit cycles here unstable, but they also have periods ranging from 31.4 h to 45.2 h. With variation in d_{bc} , a parameter proportional to the degradation rate of BC , there are Hopf bifurcations above and below the green shaded region, and no other branches of stable equilibria; see Fig. 5B. In this range of parameters, we identified a separate branch of unstable equilibria but omitted the graph because we believe it is not biologically relevant.

With the light function from Eq. (3), the mathematical model is in one of two states depending on the ZT: (during light) the production rate of P_1 is $1 + x$ times that of its free running production rate, or (during dark) the production rate of P_1 is $1 - x$ times that of its free running production rate. Treating this model in a piecewise manner

allows us to study bifurcations through Matcont, which is designed for autonomous systems. In Fig. 5C–D, we examine the same one-parameter variations as in the free running model, but now under constant light. Constant light increases the production rate of P_1 , and in Fig. 5C this effectively shifts the Hopf bifurcation point $r_1 = 0.3$ from the free running model to $r_1 = 0.23$; see panel C versus panel A. In [12], Per mutant mice maintained rhythmicity in constant light despite losing rhythmicity in constant darkness, and our model offers a new explanation of why. With the Hopf bifurcation along r_1 shifted down in the constant light model, the branch of stable limit cycles extends to lower production rates of PER.

We additionally observe that constant light conditions shift the branch of stable equilibria that starts at $r_1 = 0.8$ from Fig. 5A to start at $r_1 = 0.615$ in Fig. 5C. This stable branch is close to the green shaded region, or the parameter range of interest. In Fig. 5D, even more complex behavior arises from variation in d_{bc} . A branch of stable equilibria appears within the green shaded region, suggesting that model variables will not always converge to the stable limit cycle whose bounds are indicated by the solid orange curves.

4. Piecewise-smooth dynamics

In this section, we note the piecewise-smooth dynamics in the mathematical model. A detailed discussion of piecewise-smooth dynamical systems can be found in [55]. The function $f_0(P, I)$ for a protein P and an inhibitor I is piecewise-defined in Eq. (2). It appears in the form $f_0(BC, P_4)$ in the production rates for P_1 , REV and ROR , and in the form $f_0(S, REV)$ in the production rate for S . As a result, the dynamical system is in one of four different cases at any given time:

Case 1: $BC \leq P_4, S \leq REV$

Case 2: $BC \leq P_4, S > REV$

Case 3: $BC > P_4, S \leq REV$

Case 4: $BC > P_4, S > REV$

In Cases 1 & 2, we have $BC \leq P_4$ so that $f_0(BC, P_4) = 0$. As a result, the production rate of P_1 in Eq. (4a) is zero and the light forcing has no effect in these two cases. In Cases 1 & 3, the differential equations are linear; and in Cases 1–3, different subgroups of the model variables are decoupled. We will examine decoupling for Case 3 in Section 4.1.

We computed numerical solutions of the differential equations for r_1 between 0.1 and 1 in the free running model and observed that for $r_1 > 0.3$, the stable limit cycle passes through two or more cases. For $r_1 < 0.3$, the stable limit cycle is contained entirely in Case 3 with $BC > P_4, S \leq REV$, so we use this unique feature to study $r_1 < 0.3$ or when the production rate of P_1 is low.

4.1. Understanding Case 3

As discussed previously, there is a Hopf bifurcation in the free running model at $r_1 = 0.3$; see Fig. 5A. When $r_1 < 0.3$, numerical solutions converge to a stable equilibrium point with $BC > P_4$ and $S \leq REV$. Here, we rewrite the core circadian clock and secondary feedback loop equations to correspond to Case 3:

$$\frac{dP_1}{dt} = r_1 L(t, x)(BC - P_4) - r_2 P_1 \quad (9a)$$

$$\frac{dP_2}{dt} = r_2 P_1 - r_3 P_2 \quad (9b)$$

$$\frac{dP_3}{dt} = r_3 P_2 - r_4 P_3 \quad (9c)$$

$$\frac{dP_4}{dt} = r_4 P_3 - d_4 P_4 \quad (9d)$$

$$\frac{dREV}{dt} = r_{rev}(BC - P_4) - d_{rev} REV \quad (9e)$$

$$\frac{dROR}{dt} = r_{ror}(BC - P_4) - d_{ror} ROR \quad (9f)$$

$$\frac{dBC}{dt} = \beta_{bc} S - d_{bc} BC \quad (9g)$$

$$\frac{dS}{dt} = \beta - d_s S \quad (9h)$$

where the differential equations are linear. The steady state for the free running model with $x = 0$ is

$$Y^* = \langle P_1^*, P_2^*, P_3^*, P_4^*, REV^*, ROR^*, BC^*, S^* \rangle^T, \quad (10)$$

where

$$P_1^* = \frac{d_4}{r_2} P_4^*, \quad P_2^* = \frac{d_4}{r_3} P_4^*, \quad P_3^* = \frac{d_4}{r_4} P_4^*, \quad P_4^* = \frac{r_1}{d_4 + r_1} BC^*, \quad (11a)$$

$$REV^* = \frac{d_4 r_{rev}}{r_1 d_{rev}} P_4^*, \quad ROR^* = \frac{d_4 r_{ror}}{r_1 d_{ror}} P_4^*, \quad (11b)$$

$$BC^* = \frac{\beta_{bc}}{d_{bc}} S^*, \quad S^* = \frac{\beta}{d_s}, \quad (11c)$$

and $BC^* > P_4^*$ and $S^* \leq REV^*$ when $r_1 < 0.3$. At $r_1 = 0.3$, Y^* lies on a discontinuity boundary $S^* = REV^*$, between Cases 3 and 4, and a boundary equilibrium bifurcation [55] takes place. In Fig. 5A, we saw this bifurcation take the form of a Hopf bifurcation. To corroborate the numerical results in Fig. 5A, one can use linear stability analysis to check that Y^* is stable for $r_1 < 0.3$.

Once we introduce periodic forcing by light, a boundary equilibrium bifurcation along r_1 still exists. We observed numerically that solutions again switch from Case 3 to Case 4 at some r_1 . We let $r_1 = r_1^*(x)$ denote this boundary equilibrium bifurcation point, so that $r_1 < r_1^*(x)$ corresponds to Case 3 with $BC > P_4$ and $S \leq REV$. What is special about Case 3 is that Eqs. (9g) and (9h) for BC and S are decoupled from the rest of the model variables. We found that, while non-oscillatory in the free running model, the Case 3 equations generate oscillatory behavior in all variables besides BC and S . Eq. (11c) gives the steady state values for the decoupled system, and the eigenvalues of the Jacobian matrix are $\lambda_{1,2} = -d_{bc}, -d_s < 0$. As a result, the steady states BC^* and S^* are stable; and in Fig. 6A, example time series for BC and S in Case 3 ($x = 0.3$ and $r_1 = 0.25$) converge to the stable steady state values.

What about the other variables $\{P_i\}_{i=1}^4$, REV , and ROR ? As shown in Fig. 6A, there is still light-driven circadian variation in the rest of the model variables. To confirm our numerical results, we have used some tools from Floquet theory to study Eqs. (9a)–(9f).

Let $BC = BC^*$ and $S = S^*$ and note that the system in Eqs. (9a)–(9f),

$$U = \langle P_1, P_2, P_3, P_4, REV, ROR \rangle^T, \quad (12)$$

is of the form

$$\frac{dU}{dt} = JU + b \quad (13)$$

where J is a piecewise constant matrix and

$$b = \langle r_1 L(t, x)BC, 0, 0, 0, r_{rev}BC, r_{ror}BC \rangle^T. \quad (14)$$

The solution of this inhomogeneous system can be constructed via variation of parameters or an integrating factor approach in terms of the solution of the corresponding homogeneous problem,

$$\frac{dV}{dt} = JV. \quad (15)$$

Floquet theory can be applied to Eq. (15) to analyze the stability of the numerically observed periodic solutions of Eq. (13).

Let $J(t)$ be the piecewise Jacobian matrix of Eq. (15), with $J(t) = J_+$ if $t \bmod 24 \in [0, 12)$ and $J(t) = J_-$ if $t \bmod 24 \in [12, 24)$ where

$$J_{\pm} = \begin{bmatrix} -r_2 & 0 & 0 & -r_1(1 \pm x) & 0 & 0 \\ r_2 & -r_3 & 0 & 0 & 0 & 0 \\ 0 & r_3 & -r_4 & 0 & 0 & 0 \\ 0 & 0 & r_4 & -d_4 & 0 & 0 \\ 0 & 0 & 0 & -r_{rev} & -d_{rev} & 0 \\ 0 & 0 & 0 & -r_{ror} & 0 & -d_{ror} \end{bmatrix}. \quad (16)$$

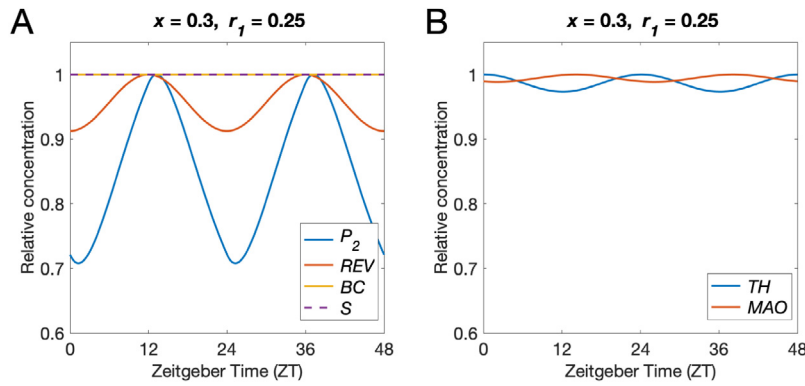


Fig. 6. Effects of decoupling in Case 3. In the mathematical model with $BC > P_4$ and $S \leq REV$, the time series of BC (panel A, yellow curve) and S (panel A, dashed purple curve) are constant, while other clock variables are oscillatory. BC activates REV (panel A, orange curve) and ROR (not graphed); as a result, REV and ROR vary by less than 10% of their peak value. Downstream of the circadian clock, TH (panel B, blue curve) and MAO (panel B, orange curve) vary minimally.

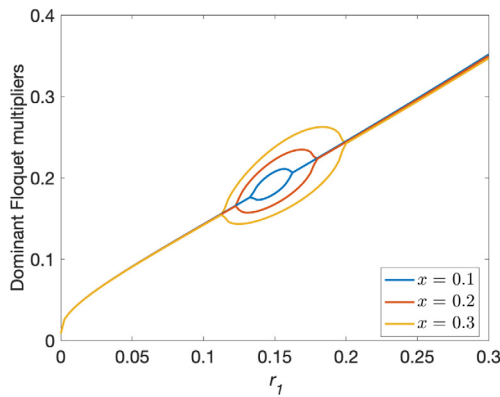


Fig. 7. Dominant Floquet multipliers for $r_1 < r_1^*(x)$. The two Floquet multipliers largest in magnitude for the model case with $BC > P_4$ and $S \leq REV$ (or $0 < r_1 < 0.3$) were computed iteratively through r_1 . Three different light amplitudes were considered: $x = 0.1$ (blue curves), $x = 0.2$ (orange curves), and $x = 0.3$ (yellow curves).

Using Floquet theory [56], the monodromy matrix is $M = e^{12J_-} e^{12J_+}$. We are interested in $r_1 < 0.3$ so that $BC > P_4$ and $S \leq REV$. Using MATLAB, we have computed the two eigenvalues of M that are largest by magnitude, ρ_1 and ρ_2 ; see Fig. 7. The eigenvalues of M are the Floquet multipliers of the dynamical system (Eqs. (9a)–(9f)). The result $|\rho_1| < 1$ predicts the limit cycle is asymptotically stable [57], as observed in the numerical simulations in Fig. 6A with BC and S converging to steady state values. Fig. 6B shows the downstream influences of this behavior on reducing the amplitudes of TH and MAO . This result has important implications for the circadian clock’s influences on dopamine, as we will discuss in the next section. Though not depicted in Fig. 7, taking large enough x can result in $|\rho_1| \geq 1$ so that the solution loses periodicity according to Floquet theory. However, in our model we treat $x > 1$ as nonphysical behavior and simply note that this separate bifurcation exists.

4.2. Physiological implications

The condition $r_1 < r_1^*(x)$ with $x > 0$ is interesting biologically because $\{P_i\}_{i=1}^4$, REV , and ROR have circadian rhythms while BC and S converge to steady state values. In the model, BC and S do not need to oscillate for the clock to generate circadian rhythms. In the Kim et al. simple model [38], the concentration of activator BMAL1-CLOCK is treated as a constant, and the solution is oscillatory anyway.

In experiments, Per mutant mice display arrhythmic activity under constant darkness and rhythms are restored under light–dark conditions [12,13]. Consistent with these results, circadian rhythms in the

free running model are abolished for $r_1 < r_1^*(0) = 0.3$ where the production rate of PER is relatively low, but become entrained in the presence of light–dark variation. The light-dependent value $r_1 = r_1^*(x)$ is the boundary equilibrium bifurcation point in the model with $BC > P_4$ and $S \leq REV$ for $r_1 < r_1^*(x)$, and takes the form of a Hopf bifurcation in the free running model (Fig. 5A). The model is intrinsically oscillatory for $r_1 > r_1^*(x)$ and not for $r_1 < r_1^*(x)$. In the presence of light–dark variation ($x > 0$), light forcing influences the intrinsic rhythms for $r_1 > r_1^*(x)$ and generates new oscillations for $r_1 < r_1^*(x)$.

Circadian variation of dopamine is essential for healthy modulation of many important physiological functions such as hunger, sleep, and mood; and abnormal rhythms exacerbate DA-related conditions such as Parkinson’s and mood disorders [58]. For $r_1 < r_1^*(x)$ in the model, the core clock variables $\{P_i\}_{i=1}^4$ display regular circadian rhythms. In contrast, TH and MAO activities vary by less than 5% (see Fig. 6B), and as a result eDA varies by less than 1% (not graphed). TH is modulated by REV and ROR , which are activated by BC ; and MAO is directly activated by BC . Therefore, it makes sense that the decoupled steady state behavior of BC when $r_1 < r_1^*(x)$ has significant downstream effects on DA. Importantly, the decoupling behavior in the model can be connected to real biological observations. Experiments in [5] have shown that circadian rhythms in Per and Cry can persist in the absence of Bmal1 and Clock rhythms. Based on our model results, the decoupling of circadian clock variables is a possible route to disrupted DA rhythms.

Bmal1 disruptions in mice have also led to arrhythmic circadian behavior in the absence of light [14,15]. Interestingly, mice with the Bmal1 deletion adapted better to light–dark variation than those without the Bmal1 deletion [15]. Yang et al. [15] propose that this is due to the absence of an intrinsic oscillator, and our model confirms this idea. Reducing Bmal1 production itself by 90% in the model results in protein levels that correspond to Case 4. This Bmal1 mutation causes the model to converge to steady state behavior in free running conditions (not shown). While decoupling does not occur in the Case 4 model, light forcing drives 24-h oscillations in clock variables with very minimal variation in S and BC . As a result, we see minimal variation in TH and MAO , and consequently in eDA .

The [15] experiments also suggest that Bmal1 deletion may be beneficial in some settings because it allows easier entrainment of mouse locomotor activity to light. Desynchronization between the internal clock and the light–dark cycle increases the risks for metabolic and cardiac dysfunction [17], so treating any clock misalignment would be beneficial in some ways. However, while Bmal1 deletion may help to restore circadian rhythms in locomotor activity with external light forcing, our model demonstrates that such a therapy could have unintended consequences, such as in dopamine regulation. Bmal1 deletion is already not ideal as it abolishes circadian variation of blood pressure [15].

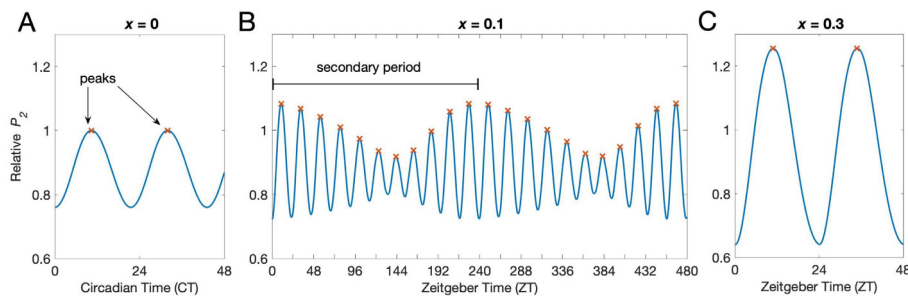


Fig. 8. Quasiperiodicity in the mathematical model. At $r_1 = 0.375$, the model dynamics changes in response to light amplitude x . The time series of P_2 for each of $x = 0$, $x = 0.1$, and $x = 0.3$ is plotted in blue in panels A–C, respectively. The peaks (or local maxima) of each curve are marked with an orange ‘x’ to help visualize periodicity. For $x = 0.1$, P_2 has a secondary frequency, which we define as the period of the peaks (panel B). The curves in all three panels are plotted relative to the peak expression of P_2 in panel A.

As in the [15] experiments, circadian rhythms in the model with $Bmal1$ disruption are eliminated in constant darkness but become entrained to light–dark variation. Experimentally, such clock behavior may be hard to distinguish from the dynamics in the Case 3 example from Fig. 6. However, it is important to draw a distinction. In Fig. 6, a low transcription rate of PER elevates $BMAL1$ -CLOCK and REV -ERBs, thereby lowering $Bmal1$ so that $S \leq REV$; and in the $Bmal1$ mutation simulated in the model, $Bmal1$ disruption is directly induced and results in lower levels of all circadian variables such that $S > REV$. Although they would appear qualitatively similar under constant dark versus light–dark experiments, these two phenotypes differ in the relationship between $Bmal1$ and REV -ERBs and may require different therapeutic targets.

The model serves as evidence that seemingly healthy circadian rhythms may have harmful downstream influences, and that the relationships between clock proteins may help to characterize the underlying dynamics. In Sections 5 and 6, we study how light input and the production rate of PER are connected to quasiperiodic and chaotic behaviors caused by misalignment in frequency.

5. Quasiperiodicity and chaos

For $r_1 > r_1^*(0) = 0.3$, the free running or intrinsic model is periodic as we have observed in Fig. 4A–B, and with $r_1 = 0.5$ the limit cycle has a period of 23.5 h. In Fig. 4C–D, the model converged to a 24-h limit cycle with sufficiently strong light forcing (with amplitude $x = 0.3$). In this section, we are interested in understanding what happens when r_1 and x are perturbed. In particular, we study some quasiperiodic and chaotic behaviors and connect these results with experimental observations.

5.1. Quasiperiodic dynamics in the core circadian clock

We observed that quasiperiodic behavior exists in the model by experimenting with r_1 and x . Quasiperiodic behavior occurs when the ratio between two frequencies of an attractor is irrational, and can be observed as trajectories winding around endlessly on a torus [59]. In Fig. 8, all three panels were computed with fixed $r_1 = 0.375$ and graphed relative to the peak in panel A. In the free running model for $r_1 = 0.375$, the time series for P_2 is 21.6-h periodic; see Fig. 8A. In Fig. 8B, we observe quasiperiodicity in which the time series displays a beat phenomenon with two frequencies, near 21.8 h and 236.5 h. Using the Wolf algorithm [51], we computed the largest Lyapunov exponent to be zero. We will further confirm quasiperiodicity in Fig. 11 later in this section. In Fig. 8C with $x = 0.3$, the model is entrained to the light–dark cycle and is 24-h periodic.

Fig. 8 suggests that r_1 and x play important roles in the periodicity of the model, and this makes sense biologically. The production rate of PER and the amplitude of light both have important roles in the periodicity of the circadian clock. Lowering clock transcription rates results in shorter period lengths [60], and changes in circadian rhythms

are dependent on light intensity [3,61]. True quasiperiodic behavior cannot be observed experimentally due to noise and measurement limitations, but quasiperiodicity is still meaningful biologically and can be characterized in experimental contexts [16,62]. It is known that weaker light intensity leads to less effective circadian entrainment in humans [61] and West et al. [17] have demonstrated that desynchrony between the external light–dark cycle and the internal clock in mice creates significant physiological disturbances. In mouse experiments by Erzberger et al. [16], changes to the period of the light–dark schedule often resulted in quasiperiodic activity patterns, and these patterns were distinguished using actograms and spectral analyses. These actograms graph periods of activity over time, and quasiperiodic patterns can be observed as phase drifting. To connect our model results with this behavior, we have visualized the time series in Fig. 9A as a model actogram, with 6 h before and after P_2 peaks indicating periods of activity. Consistent with the experiments, the quasiperiodic behaviors in the model are also observable as phase drifting. With this low production rate for PER ($r_1 = 0.375$), the model behavior does not become fully entrained to the light–dark cycle until light amplitude is increased to about $x = 0.274$; see Fig. 9B.

In our model, we further characterized periodicity across variation in r_1 and x as follows: We computed Poincaré sections containing points where P_2 has a peak (or local maximum) in each light case for $0.1 \leq r_1 \leq 1$. In Fig. 10, we plotted all P_2 peaks for 30,000 h for the four light cases. In Fig. 10A, P_2 peaks across each time series for varying r_1 line up at the same concentration, indicating that each time series is periodic. For $r_1 < 0.3$, the model variables converge to stable steady state solutions as discussed in Section 3.2, and the P_2 steady states are indicated by the dashed blue curve. In Fig. 10B–D with $x > 0$, we observe periodicity for $r_1 < r_1^*$ where the model is not intrinsically oscillatory, and this is consistent with our results in Section 4. Near $r_1 = 0.5$ in Fig. 10B, P_2 is periodic. However, the model is non-periodic in the filled-in bands, and simulations and Lyapunov exponents suggest that the P_2 time series for r_1 in those regions is similar in behavior to the example given in Fig. 8B. In Fig. 8B, we have indicated P_2 peaks with an orange ‘x’, and one can see how the P_2 peaks for $r_1 = 0.375$ in Fig. 10B correspond to the peaks observed in Fig. 8B. Computations of the largest Lyapunov exponent for each r_1 suggest quasiperiodicity across all non-periodic regions in panel B and most non-periodic regions in panels C and D with indications of chaos for few r_1 .

5.2. Downstream influences on dopamine

Both dopamine synthesis and degradation are influenced by the circadian clock, and the dopaminergic system is known to regulate mood [2,33,63]. Polymorphisms in clock genes are linked to DA-related neurological and psychiatric conditions [2]. Those with Parkinson’s disease often experience sleep and circadian disorders [64,65], and adults with ADHD often experience a lack of circadian rhythmicity [28]. Treating circadian disruptions has helped to ameliorate symptoms of depression and bipolar disorder [63].

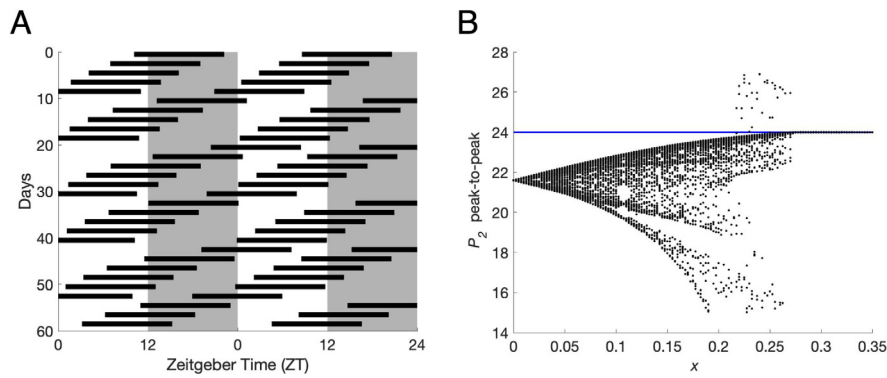


Fig. 9. Quasiperiodic patterns and dependence on light amplitude. For $r_1 = 0.375$ and $x = 0.1$ the P_2 time series from Fig. 8 is plotted as an actogram in panel A, with horizontal bars indicating 6 h before to 6 h after each P_2 peak. As in [16], quasiperiodic behavior is observed as phase drifting. In panel B, all peak-to-peak differences of the P_2 time series are plotted (black points) for varying light amplitude x . The horizontal blue line indicates 24-h periodicity.

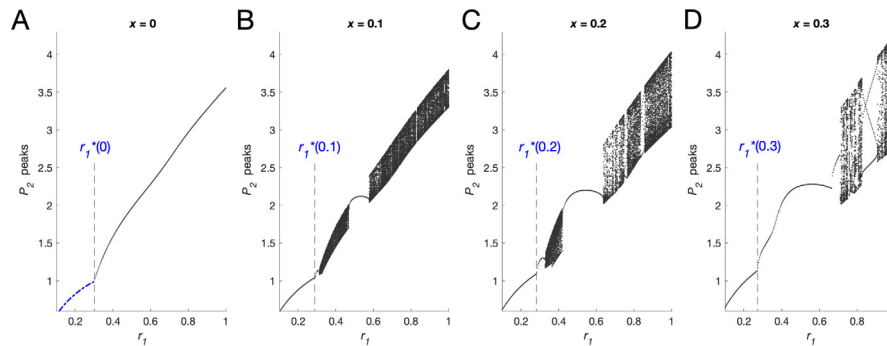


Fig. 10. Poincaré sections using peaks of P_2 . The peaks of the times series of P_2 were tracked for 30,000 h for $x = 0$ (panel A), $x = 0.1$ (panel B), $x = 0.2$ (panel C), and $x = 0.3$ (panel D). **Panel A:** In the free running model, P_2 converges to a stable limit cycle for $r_1 > r_1^*(0) = 0.3$, as in Fig. 5A. The peaks of P_2 coincide with each other, indicating the time series is periodic. For $r_1 < r_1^*(0) = 0.3$, the time series for P_2 converges to a steady state value (dashed blue curve). **Panels B–D:** For the model under the light–dark cycle, variation in r_1 leads to quasiperiodic solutions, as in Fig. 8. In panel B, all “bands” correspond to quasiperiodic regions where for each r_1 the largest Lyapunov exponent (not shown) is 0. In panels C and D, Lyapunov exponents suggest small regions of chaos within $0.65 < r_1 < 0.7$ and $0.7 < r_1 < 0.83$, respectively.

In our mathematical model, we observed some circadian disruptions in the form of quasiperiodic and chaotic behavior caused by incommensurate frequencies of the external light–dark cycle and internal clock. The parameter values in Fig. 8B generated quasiperiodic behavior in clock variables. This quasiperiodicity can be observed in downstream DA as well; see Fig. 11A–C. The peaks of eDA in Fig. 11A closely follow the peaks of TH , and the eDA time series has a secondary period close to 236.5 h. The relationship between eDA , TH , and MAO can be observed in Fig. 11B, where the model trajectory for 480 h wraps around a torus. Computations for a much longer time span show that the trajectory continues to densely wrap around the torus, supporting quasiperiodicity. Additionally, the peak to peak distances in the eDA time series fluctuate from about 20.5 to 22.5 h; see 11C. Experimentally, this could be observed as phase drifting where peak expression is gradually shifted each day, such as in non-24-h sleep–wake disorder [66].

Lyapunov exponent computations suggested chaos for particular parameter values. As discussed earlier, chaotic clock behavior has been identified in previous circadian models and has potential implications for physiology. Gonze and Goldbeter [18] have studied chaos in a circadian model consisting of a single feedback loop, and have shown that the periodic versus chaotic dynamics in their model depends strongly on the form and amplitude of light input, which influences PER transcription. Similarly, we observed in Section 5.1 that the transcription rate of Per and the light amplitude both have a significant impact on the model dynamics. To exemplify chaos in the model, we chose to look at the behavior in eDA for $x = 0.3$ and $r_1 = 0.75$. The clock’s chaotic behavior has downstream influences on eDA ; in Fig. 11D, the relative eDA time series fluctuates between 0.9 and 1 but is non-periodic. Peaks still shortly follow TH peaks, and the 3 dimensional trajectory

is graphed in panel E. Peak to peak distances vary from about 23 to 35 h (panel F), resulting in much larger disturbances to DA rhythms in relation to the 24-h light–dark cycle. Such clock behavior disrupts DA dynamics and could exacerbate DA related conditions. However, the parameter value $r_1 = 0.75$ is outside the “normal” parameter range for this model and we simply note that such chaotic behavior exists for some large perturbations in r_1 . In the next section, we measure how periodicity and quasiperiodicity depend on r_1 and d_{bc} within their “normal” ranges for various light intensities, and discuss how period homeostasis depends on light–dark variation.

6. Period homeostasis

The mammalian circadian clock is characterized by a period of about 24 h, and environmental or genetic perturbations have the potential to disrupt periodicity [67,68]. Amazingly, in many cases near-24-h rhythms can be maintained even in the absence of external cues. In the free running model, we computed period as r_1 and d_{bc} varied 25% below and 25% above their original values: $r_1 = 0.5$ and $d_{bc} = 0.3$; see Fig. 12. The filled regions indicate periodic behavior, and period varies from about 20 to 30 h across this parameter regime. Generally, as r_1 and d_{bc} move away from their original values, the period moves away from 24 h.

When the light–dark cycle is introduced, the model behavior in all of the parameter regime of interest is oscillatory; see Fig. 13A–D. For a small light amplitude ($x = 0.01$), period dependence on variations in r_1 and d_{bc} resembles that of the free running model ($x = 0$) for much of r_1 and d_{bc} . Without the light–dark forcing, the model behavior is non-oscillatory for low r_1 and low d_{bc} , but with light–dark forcing there

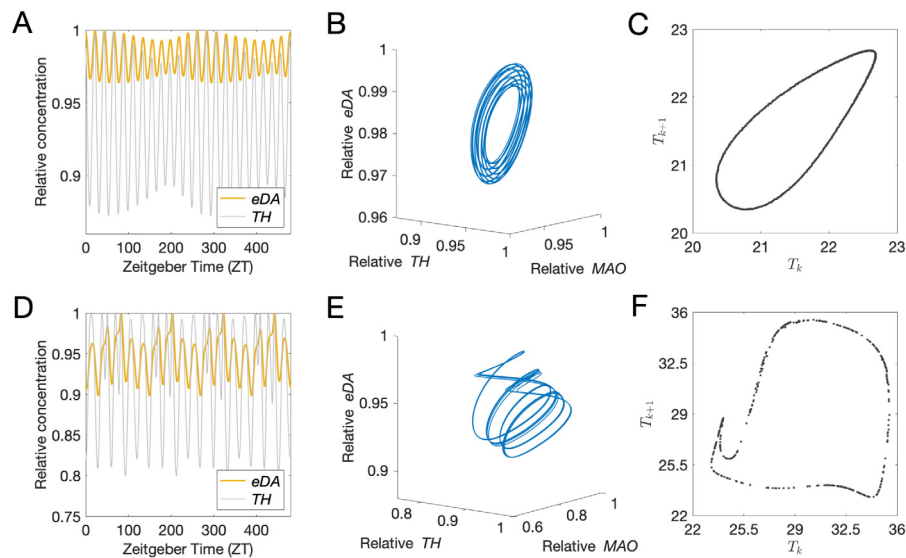


Fig. 11. Quasiperiodicity and chaos in DA dynamics. The mathematical model in this paper is connected with the extant DA model in [36] to predict extracellular DA (*eDA*) rhythms with $x = 0.1$ and $r_1 = 0.375$ (panels A-C); and $x = 0.3$ and $r_1 = 0.75$ (panels D-F). The *TH* time series (gray) in panels A and D are influenced by the quasiperiodic and chaotic behaviors of *REV*, *ROR*, and *BC*, leading to quasiperiodic and chaotic dynamics in *eDA* (yellow). Panels B and E show the trajectories of *eDA* vs. *TH* vs. *MAO* for 480 h corresponding to panels A and D, respectively. Panels C and F indicate peak to peak distances of the *eDA* time series for 18,000 h with the parameters from A and D, respectively. T_k indicates the time distance between the k th and $(k + 1)$ th peaks and T_{k+1} indicates the time distance between the $(k + 1)$ th and $(k + 2)$ th peaks. In the quasiperiodic case, the peak to peak distances fluctuate from about 20.5 to 22.5 h (panel C). In the chaotic case the peak to peak distances fluctuate from about 23 to 35 h (panel F).

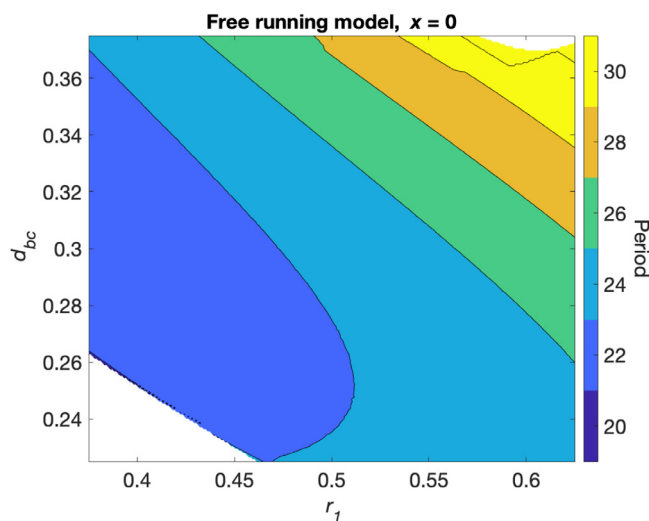


Fig. 12. Period versus r_1 and d_{bc} for the free running model. The period of the model behavior with light input $x = 0$ ranges from 20 to 30 h for r_1 and d_{bc} parameter values between 25% below and 25% above their original values. The white areas indicate steady state behaviors where the solution does not oscillate.

is an entrained oscillatory response; see lower left corners of Fig. 12 versus Fig. 13A. As in Section 5.1, external forcing drives new, 24-h oscillations in parameter regimes where the model is not intrinsically oscillatory. In Fig. 13A, the middle light blue section corresponds to 24-h oscillations, and this region expands as x increases. When $x = 0.3$, the clock has a period of 24 h everywhere; see Fig. 13D.

In Section 5, we observed some quasiperiodic behavior in the presence of light input. The quasiperiodic behaviors throughout our parameter regime of interest are characterized by a beating phenomenon like in Fig. 8B. For each r_1 and d_{bc} , we created an interpolating curve through the P_2 peaks and computed the period of this curve as the secondary period. We have plotted these values across different r_1 and d_{bc} in Fig. 13E–H for $x = 0.01$, $x = 0.1$, $x = 0.2$, and

$x = 0.3$, respectively. With a small light amplitude of $x = 0.01$, the model behavior is quasiperiodic for much of the intrinsically oscillatory parameter regime; compare the behaviors in Fig. 13A and E to that of the free running model shown in Fig. 12. In parameter regions where solutions previously converged to steady state values in the free running model, the clock is now periodic and entrained to the light–dark cycle. Secondary periods above 2^{12} hs were not computed. An infinitely long secondary period produces the same behavior as in constant amplitude oscillations. In Fig. 13E–G, we observe long but finite secondary periods in parts of the regions characterized by a 24-h primary period. Here, the model is partially entrained since the primary period is 24 h but the amplitude varies. As x is increased to 0.3, the quasiperiodicity is eliminated and the clock is fully entrained to the light–dark cycle for all r_1 and d_{bc} in the “normal” parameter regime; see Fig. 13H.

7. Conclusion

We have reduced a mathematical model of the mammalian circadian clock and its downstream influences on the dopaminergic system. The full model is detailed in [35]. The model in this paper displays near-24-h rhythmicity both with and without light input and retains key features of the circadian clock. The model is capable of different dynamics, including decoupling, quasiperiodicity, and chaos, and these behaviors can help explain experimental observations. We demonstrated that *Bmal1* and *BMAL1-CLOCK* can lose rhythmicity even when other clock variables remain periodic, and this leads to low amplitude oscillations in dopaminergic variables. We characterized quasiperiodicity and chaos in the model, showed how these dynamics influence dopamine rhythms, and discussed these results in connection with experiments and clinical observations. Also, sufficiently strong light variation helped to improve period homeostasis and reduce regions of quasiperiodicity. The model in this paper can be used to further study the impact of different light–dark conditions on the circadian clock, investigate potential disruptions in diurnal variation of DA, and explore therapeutic targets for ameliorating these disruptions. For example, experimentalists have proposed that restless legs syndrome (RLS) is characterized by increased circadian variation in dopamine metabolites

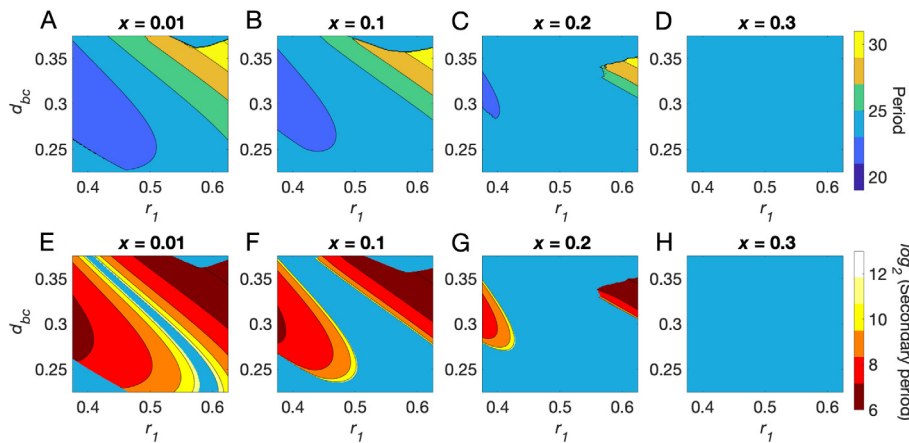


Fig. 13. Period (panels A–D) and secondary period (panels E–H) versus r_1 and d_{bc} for the model with light input. The model behavior is oscillatory for all r_1 and d_{bc} values in the parameter regime of interest (panels A–D). The model with light input has a secondary Hopf bifurcation which leads to secondary oscillations. Secondary period computations (\log_2 scale) versus r_1 and d_{bc} are plotted in panels E–H. Secondary periods above $2^{12} = 4096$ h were not computed. Light blue regions in panels E–H indicate either secondary periods above 4096 h or no quasiperiodicity. As the light input x is increased from left to right, the solution becomes entrained to the light–dark cycle, with period 24 h, for a larger range of parameter values (panels A–D). At $x = 0.3$, the model behavior is fully entrained with no secondary oscillations (panel H).

and low levels of iron, a cofactor for TH [29,69,70]. Dopaminergic treatments help relieve RLS symptoms [71]. The mathematical model studied in this paper could be used to investigate the pathophysiology and treatment of conditions like RLS that are linked to both circadian rhythms and the dopaminergic system. In addition, there is evidence that the dopaminergic system reciprocally affects the circadian clock [72–74]. Extending the model to consider these findings will be the subject of future work.

Declaration of competing interest

The authors declare that they have no known competing financial interests or personal relationships that could have appeared to influence the work reported in this paper.

Acknowledgment

The authors gratefully acknowledge helpful comments from Michael C. Reed.

Appendix. The condition to avoid finite-time blow-up

Here, we calculate a condition for proper stabilization of S . In some simulations of system ((4)a–h), blow-up behavior was observed, with concentrations diverging as a finite critical time is approached, $t \rightarrow t_c$. Numerical results showed that S would grow most rapidly, followed by BC and others. To understand how to avoid this unphysical behavior, we analyze this class of dynamics in the model.

The dominance of S and BC in these dynamics allow us to restrict attention to Case 4 ($S > REV$ and $BC > P_4$) from Section 4. We will show that the driving influence of S motivates re-arranging the system in the ordering

$$\frac{dS}{dt} + d_s S = \alpha(S - REV)ROR + \beta \tag{A.1a}$$

$$\frac{dBC}{dt} + d_{bc} BC = \beta_{bc} S \tag{A.1b}$$

$$\frac{dROR}{dt} + d_{ror} ROR = r_{ror}(BC - P_4) \tag{A.1c}$$

$$\frac{dREV}{dt} + d_{rev} REV = r_{rev}(BC - P_4) \tag{A.1d}$$

$$\frac{dP_1}{dt} + r_2 P_1 = r_1 L(t, x)(BC - P_4) \tag{A.1e}$$

$$\frac{dP_2}{dt} + r_3 P_2 = r_2 P_1 \tag{A.1f}$$

$$\frac{dP_3}{dt} + r_4 P_3 = r_3 P_2 \tag{A.1g}$$

$$\frac{dP_4}{dt} + d_4 P_4 = r_4 P_3. \tag{A.1h}$$

Each of Eqs. ((A.1)b–h) can individually be viewed as a linear first order rate equation, with an inhomogeneous forcing due to other species and general solution of the form:

$$\frac{dU}{dt} + kU = F(t) \implies U(t) = Ce^{-kt} + e^{-kt} \int_0^t F(\tau)e^{k\tau} d\tau. \tag{A.2}$$

For a singular forcing term, $F(t) = A/(t_c - t)^\gamma$ as $t \rightarrow t_c$ with $\gamma > 1$, we can use the asymptotics of the exponential integral special function [75, Chap 6] to obtain the leading order estimate of the solution as

$$U(t) \sim \frac{A}{\gamma - 1} (t_c - t)^{-\gamma+1} \quad \text{as } t \rightarrow t_c. \tag{A.3}$$

This can also be interpreted as $U(t)$ being dominated by the particular solution term, and to leading order can be written as $U(t) \sim \int F(t) dt$ for any γ . The integration means that the solution is less singular than its forcing term. Consequently, the ordering of ((A.1)a–h) arranges the solutions from most to least singular:

$$S \gg BC \gg \{REV, ROR, P_1\} \gg P_2 \gg P_3 \gg P_4 \quad \text{as } t \rightarrow t_c.$$

This justifies the further simplifications $S - REV \sim S$ and $BC - P_4 \sim BC$.

The equation for S is special because there S also appears in a nonlinear forcing term. If we assume the form $S(t) \sim C/(t_c - t)^k$ with $k > 2$ then integrating equation ((A.1)b–d) we get

$$BC = O((t_c - t)^{-k+1}) \quad REV = O((t_c - t)^{-k+2}) \quad ROR = O((t_c - t)^{-k+2}).$$

Then the dominant terms of ((A.1)a) reduce to

$$\frac{dS}{dt} = \alpha SROR$$

and substituting in the power-law forms for S, REV yields a balance for the exponent, $-k - 1 = -k - k + 2$. This yields $k = 3$, justifying our earlier assumptions and giving the overall blow-up behavior,

$$S = O((t_c - t)^{-3}), \quad BC = O((t_c - t)^{-2}), \quad \{REV, ROR, P_1\} = O((t_c - t)^{-1}), \\ P_2 = O(\ln(t_c - t)), \quad P_3 = O((t_c - t) \ln(t_c - t)), \quad P_4 = O((t_c - t)^2 \ln(t_c - t)).$$

Having justified that in blow-up, $S \gg REV \gg 1$, returning to ((A.1)a), we can re-write this equation as

$$\frac{dS}{dt} = (\alpha ROR - d_s)S + o(S). \tag{A.4}$$

Considering the sign of the linear growth term, we see that $S(t)$ will be monotone increasing and grow without bound if the coefficient in this

term is positive. Therefore, to avoid the possibility of generating this blow-up behavior, we require that

$$ROR(t) < \frac{d_s}{\alpha}. \quad (\text{A.5})$$

References

- [1] C.S. Colwell, Linking neural activity and molecular oscillations in the scn, *Nat. Rev. Neurosci.* 12 (10) (2015) 553–569.
- [2] U. Albrecht, Molecular mechanisms in mood regulation involving the circadian clock, *Front. Neurol.* 8 (30) (2017) 1–6.
- [3] J.A. Ripperger, C. Jud, U. Albrecht, The daily rhythm of mice, *FEBS Lett.* 585 (2011) 1384–1392.
- [4] D.B. Forger, *Biological Clocks, Rhythms, and Oscillations*, The MIT Press, Cambridge, Massachusetts, 2017.
- [5] N. Preitner, F. Damiola, L.-L. Molina, J. Zakany, D. Duboule, U. Albrecht, U. Schibler, The orphan nuclear receptor rev-erb alpha controls circadian transcription within the positive limb of the mammalian circadian oscillator, *Cell* 110 (2002) 251–260.
- [6] J. Lee, S. Lee, S. Chung, N. Park, G.H. Son, H. An, J. Jang, D.-J. Chang, Y.-G. Suh, K. Kim, Identification of a novel circadian clock modulator controlling bmal1 expression through a ror/rev-erb-response element-dependent mechanism, *Biochem. Biophys. Res. Commun.* 469 (2016) 580–586.
- [7] D.B. Forger, C.S. Peskin, A detailed predictive model of the mammalian circadian clock, *Proc. Natl. Acad. Sci. USA* 100 (25) (2003) 14806–14811.
- [8] J.-C. Leloup, A. Goldbeter, Toward a detailed computational model for the mammalian circadian clock, *Proc. Natl. Acad. Sci. USA* 100 (12) (2003) 7051–7056.
- [9] C.I. Hong, E.D. Conrad, J.J. Tyson, A proposal for robust temperature compensation of circadian rhythms, *Proc. Natl. Acad. Sci. USA* 104 (4) (2007) 1195–1200.
- [10] J. Garcia-Ojalvo, M.B. Elowitz, S.H. Strogatz, Modeling a synthetic multicellular clock: Repressilators coupled by quorum sensing, *Proc. Natl. Acad. Sci. USA* 101 (30) (2004) 10955–10960.
- [11] S.H. Strogatz, From kuramoto to crawford: exploring the onset of synchronization in populations of coupled oscillators, *Physica D* 143 (2000) 1–20.
- [12] S. Steinlechner, B. Jacobmeier, F. Scherbarth, H. Dernbach, F. Kruse, U. Albrecht, Robust circadian rhythmicity of per1 and per2 mutant mice in constant light, and dynamics of per1 and per2 gene expression under long and short photoperiods, *J. Biol. Rhythms* 17 (3) (2002) 202–209, <http://dx.doi.org/10.1177/074873040201700303>.
- [13] B. Zheng, D.W. Larkin, U. Albrecht, Z.S. Sun, M. Sage, G. Eichele, C.C. Lee, A. Bradley, The mper2 gene encodes a functional component of the mammalian circadian clock, *Nature* 400 (6740) (1999) 169–173, <http://dx.doi.org/10.1038/22118>.
- [14] S.N. Haque, S.R. Booreddy, D.K. Welsh, Effects of bmal1 manipulation on the brain's master circadian clock and behavior, *Yale J. Biol. Med.* 92 (2019) 251–258.
- [15] G. Yang, L. Chen, J. Zhang, B. Ren, G.A. FitzGerald, Bmal1 deletion in mice facilitates adaptation to disrupted light/dark conditions, *JCI Insight* 4 (10) (2019) 1–8, <http://dx.doi.org/10.1172/jci.insight.125133>.
- [16] A. Erzberger, G. Hampp, A.E. Granada, U. Albrecht, H. Herzog, Genetic redundancy strengthens the circadian clock leading to a narrow entrainment range, *J. R. Soc. Interface* 10 (20130221) (2013) 1–11.
- [17] A.C. West, L. Smith, D.W. Ray, A.S.I. Loudon, T.M. Brown, D.A. Bechtold, Misalignment with the external light environment drives metabolic and cardiac dysfunction, *Nature Commun.* 8 (417) (2017) 1–10.
- [18] D. Gonze, A. Goldbeter, Entrainment versus chaos in a model for a circadian oscillator driven by light-dark cycles, *J. Stat. Phys.* 101 (1/2) (2000) 649–663.
- [19] G. Kurosawa, A. Goldbeter, Amplitude of circadian oscillations entrained by 24-h light-dark cycles, *J. Theoret. Biol.* 242 (2) (2006) 478–488, <http://dx.doi.org/10.1016/j.jtbi.2006.03.016>.
- [20] J.D. Caluwe, J.R.F. de Melo, A. Tosenberger, C. Hermans, N. Verbruggen, J.-C. Leloup, D. Gonze, Modeling the photoperiodic entrainment of the plant circadian clock, *J. Theoret. Biol.* 420 (2017) 220–231.
- [21] D. Battogtokh, J.J. Tyson, Deciphering the dynamics of interlocked feedback loops in a model of the mammalian circadian clock, *Biophys. J.* 115 (2018) 2055–2066.
- [22] R. Wise, Dopamine, learning and motivation, *Nat. Rev. Neurosci.* 5 (2004) 1–12.
- [23] W. Schultz, Multiple reward signals in the brain, *Nat. Rev. Neurosci.* 1 (2000) 199–207.
- [24] J. Lotharius, P. Brundin, Pathogenesis of parkinson's disease: dopamine vesicles and alpha-synuclein, *Nat. Rev. Neurosci.* 3 (2002) 932–942.
- [25] F.T.A. A. Graybiel, M. Kimura, The basal ganglia in adaptive motor control, *Science* 265 (1994) 1826–1831.
- [26] T. Kienast, A. Heinz, Dopamine in the diseased brain, *CNS Neurol. Disord. Drug Targets* 5 (2006) 109–131.
- [27] I.N. Karatsoreos, Links between circadian rhythms and psychiatric disease, *Frot. Behav. Neurosci.* 8 (162) (2014) 1–5.
- [28] A. Baird, A. Coogan, A. Siddiqui, R. Donev, J. Thome, Adult attention-deficit hyperactivity disorder is associated with alterations in circadian rhythms at the behavioural, endocrine and molecular levels, *Mol. Psychiatry* 17 (2012) 988–995.
- [29] C.J. Earley, K. Hyland, R.P. Allen, Circadian changes in csf dopaminergic measures in restless legs syndrome, *Sleep Med.* 7 (2006) 263–268.
- [30] E. Ikeda, N. Matsunaga, K. Kakimoto, K. Hamamura, A. Hayashi, S. Koyanagi, S. Ohdo, Molecular mechanism regulating 24-hour rhythm of dopamine d3 receptor expression in mouse ventral striatum, *Mol. Pharmacol.* 83 (2013) 959–967.
- [31] S. Chung, E.J. Lee, S. Yun, H.K. Choe, S.-B. Park, H.J. Son, K.-S. Kim, D.E. Dluzen, I. Lee, O. Hwang, G.H. Son, K. Kim, Impact of circadian nuclear receptor rev-erb alpha on midbrain dopamine production and mood regulation, *Cell* 157 (2014) 858–868.
- [32] E.P. Sleipness, B.A. Sorg, H.T. Jansen, Diurnal differences in dopamine transporter and tyrosine hydroxylase levels in rat brain: Dependence on the suprachiasmatic nucleus, *Brain Res.* 1129 (2007) 34–42.
- [33] G. Hampp, J.A. Ripperger, T. Houben, I. Schmutz, C. Blex, S. Perreau-Lenz, I. Brunk, R. Spanagel, G. Ahnert-Hilger, J.H. Meijer, U. Albrecht, Regulation of monoamine oxidase a by circadian-clock components implies clock influence on mood, *Curr. Biol.* 18 (2008) 678–683.
- [34] T.R. Castaneda, B. Marquez de Prado, D. Prieto, F. Mora, Circadian rhythms of dopamine, glutamate and gaba in the striatum and nucleus accumbens of the awake rat: modulation by light, *J. Pineal Res.* 36 (3) (2004) 177–185.
- [35] R. Kim, M.C. Reed, A mathematical model of circadian rhythms and dopamine, *Theor. Biol. Med. Model.* 18 (8) (2021) 1–15.
- [36] J.A. Best, H.F. Nijhout, M.C. Reed, Homeostatic mechanisms in dopamine synthesis and release: a mathematical model, *Theor. Biol. Med. Model.* 6 (21) (2009) 1–20.
- [37] N.E. Buchler, M. Louis, Molecular titration and ultrasensitivity in regulatory networks, *J. Mol. Biol.* 384 (5) (2008) 1106–1119.
- [38] J.K. Kim, D.B. Forger, A mechanism for robust circadian timekeeping via stoichiometric balance, *Mol. Syst. Biol.* 8 (630) (2012) 1–14.
- [39] M. Zhou, J.K. Kim, G.W.L. Eng, D.B. Forger, D.M. Virshup, A period2 phospho-switch regulates and temperature compensates circadian period, *Mol. Cell* 60 (2015) 77–88.
- [40] R. Narasimamurthy, S.R. Hunt, Y. Luc, J.-M. Fustin, H. Okamura, C.L. Partch, D.B. Forger, J.K. Kim, D.M. Virshup, Ckl1/e protein kinase primes the per2 circadian phosphoswitch, *Proc. Natl. Acad. Sci.* 115 (23) (2018) 5986–5991.
- [41] D.A. Golombek, R.E. Rosenstein, Physiology of circadian entrainment, *Physiol. Rev.* 90 (2009) 1063–1102.
- [42] T.A. Bedrosian, R.J. Nelson, Timing of light exposure affects mood and brain circuits, *Transl. Psychiatry* 7 (2015) 1–9, (e1017).
- [43] T.K. Sato, S. Panda, L.J. Miraglia, T.M. Reyes, R.D. Rudic, P. McNamara, K.A. Naik, G.A. FitzGerald, S.A. Kay, J.B. Hogenesch, A functional genomics strategy reveals rora as a component of the mammalian circadian clock, *Neuron* 43 (2004) 527–537.
- [44] P. Glendinning, *Stability, Instability and Chaos: An Introduction to the Theory of Nonlinear Differential Equations*, Cambridge University Press, 1994.
- [45] D. Jordan, P. Smith, *Nonlinear Ordinary Differential Equations: An Introduction for Scientists and Engineers*, Oxford University Press, 2007.
- [46] L.A. Solt, Y. Wang, S. Banarjee, T. Hughes, D.J. Kojetin, T. Lundasen, Y. Shin, J. Liu, M.D. Cameron, R. Noel, S.-H. Yoo, J.S. Takahashi, A.A. Butler, T.M. Kamenecka, T.P. Burris, Regulation of circadian behavior and metabolism by synthetic rev-erb agonists, *Nature* 485 (7396) (2013) 62–68.
- [47] M. Oleksiak, G. Churchill, D. Crawford, Variation in gene expression within and among natural populations, *Nature Genet.* 32 (2002) 261–266.
- [48] S. Boeuf, J. Keijer, N. Hal, S. Klaus, Individual variation of adipose gene expression and identification of covariated genes by cdna microarrays, *Physiol. Genomics* 11 (2002) 31–36.
- [49] A. Sigal, R. Milo, A. Cohen, N. Geva-Zatorsky, Y. Klein, Y. Liron, N. Rosenfeld, T. Danon, N. Perzov, U. Alon, Variability and memory of protein levels in human cells, *Nat. Lett.* 444 (2006) 643–646.
- [50] N.E. Buchler, F.R. Cross, Protein sequestration generates a flexible ultrasensitive response in a genetic network, *Mol. Syst. Biol.* 5 (272) (2009) 1–7.
- [51] A. Wolf, J.B. Swift, H.L. Swinney, J.A. Vastano, Determining lyapunov exponents from a time series, *Physica D* 16 (3) (1985) 285–317.
- [52] J.S. Takahashi, Transcriptional architecture of the mammalian circadian clock, *Nat. Rev. Genet.* 18 (3) (2017) 164–179.
- [53] B. Bano-Otalora, F. Martial, C. Harding, D.A. Bechtold, A.E. Allen, T.M. Brown, M.D.C. Belle, R.J. Lucas, Bright daytime light enhances circadian amplitude in a diurnal mammal, *Proc. Natl. Acad. Sci. U S A* 118 (22) (2021) 1–9, <http://dx.doi.org/10.1073/pnas.2100094118>.
- [54] Y. Lee, R. Chen, H. min Lee, C. Lee, Stoichiometric relationship among clock proteins determines robustness of circadian rhythms, *J. Biol. Chem.* 286 (9) (2011) 7033–7042.
- [55] M. di Bernardo, C. Budd, A. Champneys, P. Kowalczyk, *Piecewise-smooth dynamical systems: Theory and applications*, in: 163 of Applied Mathematical Sciences, Springer, 2008.
- [56] C. Chicone, *Ordinary differential equations with applications*, in: *Texts in Applied Mathematics*, Springer, New York, 2008, <https://books.google.com/books?id=DiMFCAAQBAJ>.

- [57] G. Teschl, Ordinary differential equations and dynamical systems, in: Graduate Studies in Mathematics, American Mathematical Society, 2012, <https://books.google.com/books?id=FZOCAQAAQBAJ>.
- [58] J. Kim, S. Jang, H.K. Choe, S. Chung, G.H. Son, K. Kim, Implications of circadian rhythm in dopamine and mood regulation, *Mol. Cells* 40 (7) (2017) 450–456.
- [59] S.H. Strogatz, *Nonlinear Dynamics and Chaos*, Perseus Books Publishing, 1994.
- [60] C. Dibner, D. Sage, M. Unser, C. Bauer, T. d'Eysmond, F. Naef, U. Schibler, Circadian gene expression is resilient to large fluctuations in overall transcription rates, *Embo J.* 28 (2009) 123–134.
- [61] R.A. Wever, J. Poláček, C.M. Wildgruber, Bright light affects human circadian rhythms, *Pflügers Archiv.* 396 (1983) 85–87.
- [62] J.A. Glazier, A. Libchaber, Quasi-periodicity and dynamical systems: An experimentalist's view, *IEEE Trans. Circuits Syst.* 35 (7) (1988) 790–809.
- [63] W.H. Walker, J.C. Walton, A.C. DeVries, R.J. Nelson, Circadian rhythm disruption and mental health, *Transl. Psychiatry* 10 (28) (2020) 1–13.
- [64] A. Videnovic, D. Golombek, Circadian and sleep disorders in parkinson's disease, *Exp. Neurol.* 243 (2013) 45–56.
- [65] D.P. Breen, R. Vuono, U. Nawarathna, K. Fisher, J.M. Shneerson, A.B. Reddy, R.A. Barker, Sleep and circadian rhythm regulation in early parkinson disease, *JAMA Neurol.* 71 (5) (2014) 589–595.
- [66] A. Goldbeter, J.-C. Leloup, From circadian clock mechanism to sleep disorders and jet lag: Insights from a computational approach, *Biochem. Pharmacol.* 191 (114482) (2021) 1–16.
- [67] P. Kim, H. Oster, H. Lehnert, S.M. Schmid, N. Salamat, J.L. Barclay, E. Maronde, W. Inder, O. Rawashdeh, Coupling the circadian clock to homeostasis: The role of period in timing physiology, *Endocr. Rev.* 40 (1) (2018) 66–95, <http://dx.doi.org/10.1210/er.2018-00049>, [arXiv:https://academic.oup.com/edrv/article-pdf/40/1/66/27202026/er.2018-00049.pdf](https://academic.oup.com/edrv/article-pdf/40/1/66/27202026/er.2018-00049.pdf).
- [68] S.A. Brown, U. Schibler, The ins and outs of circadian timekeeping, *Curr. Opin. Genet. Dev.* 9 (5) (1999) 588–594, [http://dx.doi.org/10.1016/s0959-437x\(99\)00009-x](http://dx.doi.org/10.1016/s0959-437x(99)00009-x).
- [69] D. Garcia-Borreguero, O. Larrosa, Y. de la Llave, Circadian aspects in the pathophysiology of the restless legs syndrome, *Sleep Med.* 3 (2002) S17–S21.
- [70] P.C. Baier, C. Trenkwalder, Circadian variation in restless legs syndrome, *Sleep Med.* 8 (2007) 645–650.
- [71] C. Trenkwalder, W. Paulus, A.S. Walters, The restless legs syndrome, *Lancet* 4 (8) (2005) 465–475.
- [72] K. Fifel, J. Vezoli, K. Dzahini, B. Claustrat, V. Leviel, H. Kennedy, E. Procyk, O. Dkhissi-Benyahya, C. Gronfier, H.M. Cooper, Alteration of daily and circadian rhythms following dopamine depletion in mptp treated non-human primates, *PLoS One* 9 (1) (2014) e86240, <http://dx.doi.org/10.1371/journal.pone.0086240>, <https://pubmed.ncbi.nlm.nih.gov/24465981>.
- [73] L. Gravotta, A.M. Gavrilu, S. Hood, S. Amir, Global depletion of dopamine using intracerebroventricular 6-hydroxydopamine injection disrupts normal circadian wheel-running patterns and period2 expression in the rat forebrain, *J. Mol. Neurosci.* 45 (2) (2011) 162–171, <http://dx.doi.org/10.1007/s12031-011-9520-8>.
- [74] S. Hood, P. Cassidy, M.-P. Cossette, Y. Weigl, M. Verwey, B. Robinson, J. Stewart, S. Amir, Endogenous dopamine regulates the rhythm of expression of the clock protein per2 in the rat dorsal striatum via daily activation of d2 dopamine receptors, *J. Neurosci.* 30 (42) (2010) 14046–14058, <http://dx.doi.org/10.1523/JNEUROSCI.2128-10.2010>, [arXiv:https://www.jneurosci.org/content/30/42/14046.full.pdf](https://www.jneurosci.org/content/30/42/14046.full.pdf), <https://www.jneurosci.org/content/30/42/14046>.
- [75] C. Bender, S. Orszag, *Asymptotic Methods and Perturbation Theory*, Springer-Verlag, New York, 1999.